Available online at www.sciencedirect.com
ScienceDirect
Journal of the European Ceramic Society 30 (2010) 889–897
www.elsevier.com/locate/jeurceramsoc

Thermal stability of nanostructured 13 wt% Al_2O_3–8 wt% Y_2O_3–ZrO_2 thermal barrier coatings

Qinghe Yu, Chungen Zhou *, Huiyan Zhang, Feng Zhao

Key Laboratory of Aerospace Materials and Performance (Ministry of Education), Department of Materials Science and Engineering, Beijing University of Aeronautics and Astronautics, Beijing 100191, China

Received 13 April 2009; received in revised form 20 September 2009; accepted 8 October 2009
Available online 5 November 2009

Abstract

Nanostructured 13 wt% Al_2O_3–8 wt% Y_2O_3–ZrO_2 (13AlYSZ) coatings were developed by atmospheric plasma spraying (APS). The phase structure and the morphology of the 13AlYSZ coatings were characterized using X-ray diffraction (XRD), scanning electron microscope (SEM) and transmission electron microscope (TEM). It was found that the as-sprayed coatings mainly consisted of tetragonal zirconia, with the Al element solid solution in ZrO_2. Heat treatment at 1100 °C increased the average grain size of the ZrO_2 phase from 61 to 120 nm and decreased the porosity from 23.8 to 18%. The addition of the nano-Al_2O_3 can effectively inhibit the grain growth of the zirconia phase. The mechanism on inhibiting the grain growth of nanostructured 8 wt% Y_2O_3–ZrO_2 thermal barrier coatings has been discussed in detail.

Keywords: Thermal barrier coatings; Nanostructured Al_2O_3–Y_2O_3–ZrO_2; Grain growth; Porosity; Thermal properties

1. Introduction

Thermal barrier coatings (TBCs) made of ZrO_2 stabilized by 7–8 wt% Y_2O_3 are widely used in gas turbines,[1–6] the use of TBCs has allowed higher engine operating temperatures, which has resulted in new materials issues, particularly in the context of TBCs for aircraft engines.[2] So the traditional micron coatings with laminar layers are difficult to meet the increasing demand for applications such as aerospace industry. Then nanostructured ceramic coatings were developed,[7–9] with low thermal conductivity, high coefficient of thermal expansion and excellent mechanical properties.[8–14] However, solid-state phase transformations of the nanostructured zirconia coating often occur and the grains tend to grow at high temperature. Padture et al.[15] have investigated the effects of Al_2O_3 concentration on the ZrO_2–Y_2O_3 phase stabilization at 1400 and 1500 °C, demonstrating that Al^{3+}, in addition to Y^{3+}, is soluted in ZrO_2, which can leads to the stabilization of t-ZrO_2 and c-ZrO_2, and heat treatment results in precipitate of α-Al_2O_3 particles in the coating. Zhou et al.[16] have also studied the influence of heat treatment on the grain growth of the nanostructured YSZ coating. The results showed that the average grain size increased with the rising of annealing temperature and time. The increasing of the grain size led to the decrease in the thermal insulation and thermal cycling life.[17,18] Therefore, inhibiting the grain growth at the high temperature is very important. It has been known that the dispersions of second-phase particles can inhibit grain growth by exerting a pinning force on migrating grain boundaries during thermal treatment.[19,20] However, investigation on inhibiting the grain growth of nanostructured 8 wt% Y_2O_3–ZrO_2 thermal barrier coatings through addition of nano-Al_2O_3 particles has not been reported so far.

With the above background, nano-Al_2O_3 particles were added into plasma sprayed nanostructured YSZ coating in this paper. The influence of heat treatment on the grain growth and porosity of the 13 wt% Al_2O_3–8 wt% Y_2O_3–ZrO_2 (13AlYSZ) coating were studied. And the mechanism on inhibiting the grain growth of nanostructured 8 wt% Y_2O_3–ZrO_2 thermal barrier coatings has been investigated for providing the relevant knowledge.

2. Experimental procedures

The original 13 wt% Al_2O_3–8 wt% Y_2O_3–ZrO_2 (13AlYSZ) powder is composed of nanostructured 8 wt% Y_2O_3–ZrO_2

* Corresponding author. Tel.: +86 10 82338622; fax: +86 10 82338200.
E-mail addresses: yqh@mse.buaa.edu.cn (Q. Yu), cgzhou@buaa.edu.cn (C. Zhou).

0955-2219/$ – see front matter © 2009 Elsevier Ltd. All rights reserved.
doi:10.1016/j.jeurceramsoc.2009.10.005

(8YSZ) and Al_2O_3 (Nanjing High Technology Nano Company of China). The average size of 8YSZ and Al_2O_3 particle is 30 and 20 nm, respectively. The individual nano-particle is so fine that cannot be used for plasma spray. Before spraying finely dispersed particles must be agglomerated to size about 30–100 μm. A particle size distribution around 50 μm was used in this study.

The 13 wt% Al_2O_3–8 wt% Y_2O_3–ZrO_2 (13AlYSZ) powder was sprayed on the stainless steel. The parameters for plasma spraying have been reported in our previous study.[16] The temperature of the substrate and coating during the plasma spraying was about 300–400 °C because of air cooling. It was measured using a thermal couple placed in the back of the sample. Then, the sample used for annealing was put in cold water immediately after the air plasma spraying. The coating detached from the stainless steel was 1 mm in thickness.

The heat-treatment tests of the free-standing coatings were performed at 1100 °C for 25, 100 and 300 h, respectively.

The original zirconia powders and the heat-treated coatings were characterized using a D/max 2200pc X-ray diffractometer (Cu Kα radiation; Rigaku, Tokyo, Japan). The energy dispersive X-ray spectroscopy (EDXS) was used to determine the composition of the coatings. Particle morphology observation and crystal structure determination were also done on an analytical transmission electron microscope (TEM). The porosity of the 13AlYSZ coatings was tested by Mercury porosimetry method, using an autopore II 9220 V3.04. Before the measurement, specimen surfaces were finely polished in order to minimize the effect of surface roughness to the porosity measurement.

3. Experimental results

3.1. Microstructure of the as-sprayed nanostructured 13AlYSZ coatings

Fig. 1 illustrates the XRD patterns of the original powder and the as-sprayed 13AlYSZ coatings. As shown in Fig. 1(a), the original nano-powders are composed of m-ZrO_2, t-ZrO_2 and α-Al_2O_3. Fig. 1(b) is the XRD spectrum of the as-sprayed 13AlYSZ nanostructured TBCs. In the as-sprayed zirconia, metastable t-ZrO_2 is the main phase, no m-ZrO_2 phase and α-Al_2O_3 are observed. The t-ZrO_2 is thought to form due to the rapid quenching of droplet after impacting on the substrate during plasma spraying. The absence of α-Al_2O_3 can be explained by the solid solution of Al atoms in ZrO_2 during plasma spraying.[15,21] The undoped coating exhibits only tetragonal t (0 0 4) and t (4 0 0) peaks at $2\theta = 73.4°$, 74.4° at higher magnifications of XRD pattern, while the tetragonal peak of coating doped with 8 wt% Al_2O_3 tends to shift. Similar results have been found.[22] This phenomenon means that Al_2O_3 is dissolved in the matrix and acts as a stabilizer like Y_2O_3.

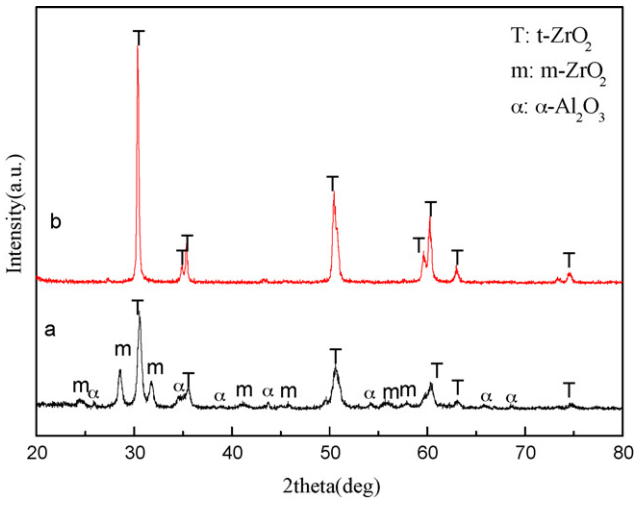

Fig. 1. XRD patterns of original powder (a) and as-sprayed 13AYSZ coatings (b).

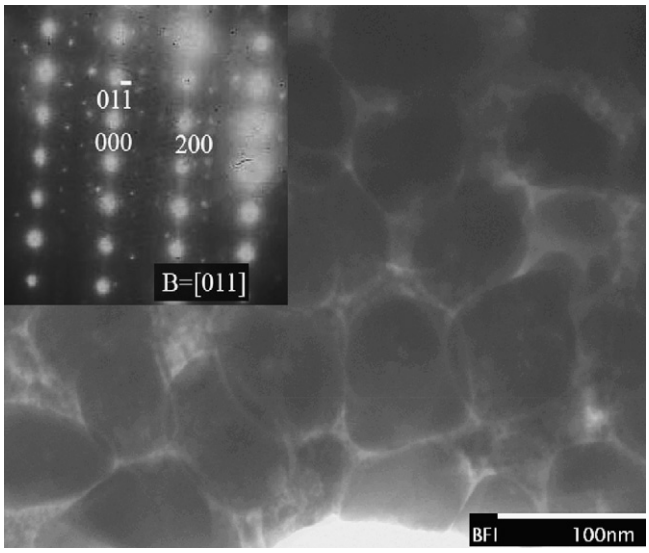

Fig. 2. TEM morphology of the as-sprayed nanostructured 13AlYSZ coating.

TEM morphology of the as-sprayed nanostructured 13AlYSZ coating is shown in Fig. 2. The TEM pictures of the 13AlYSZ coating show the regions of unmelted particles, because the melted area in the TEM exists as continuous integrity, with no clear boundaries. Obviously, the grain size is about 60 nm. The selected area electron diffraction pattern (SAEDP) along [0 1 1] direction confirms the t-ZrO_2 phase in the as-sprayed coating.

3.2. Grain growth of heat-treated nanostructured 13AlYSZ coatings

Fig. 3 shows the XRD patterns of as-deposited coatings before and after annealing treatment at 1100 °C for 25, 100 and 300 h. The coatings before and after annealing treatment consist of single t-ZrO_2, indicating that no phase transformation occur during the annealing. After annealing treatment at 1100 °C for 100 and 300 h, the α-Al_2O_3 phase appears. Moreover, the increasing intensities of α-Al_2O_3 phase imply that more α-Al_2O_3 phase is precipitated with longer annealing time. The mean grain sizes of the matrix t-ZrO_2 phase in heat-treated coat-

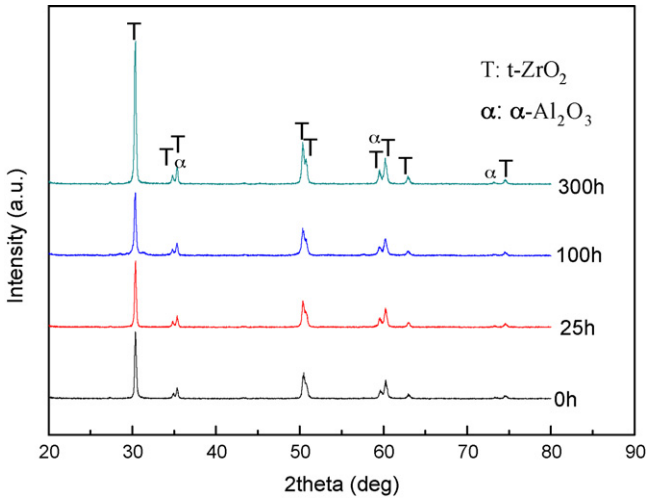

Fig. 3. XRD patterns of as-deposited 13AlYSZ coatings before and after annealing treatment at 1100 °C for 25, 100 and 300 h.

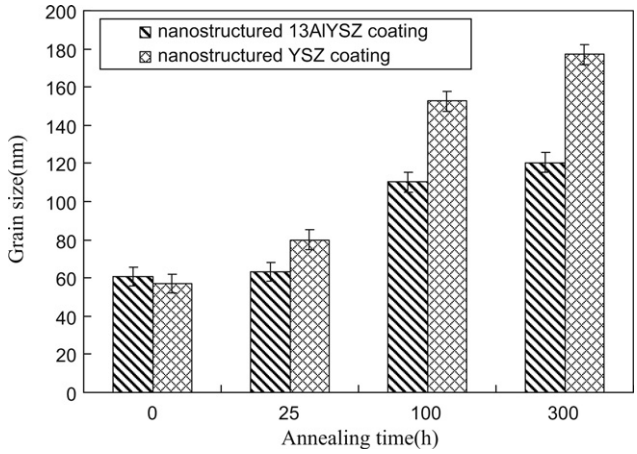

Fig. 4. Comparison of the grain size of the as-sprayed nanostructured 13AlYSZ and nanostructured YSZ coatings.

ings were roughly estimated using the Scherrer equation[23,24]:

$$B_p(2\theta) = \frac{0.9\lambda}{D\cos\theta} \quad (1)$$

where D is the average dimension of crystallite, B_p (2θ) the broadening of the diffraction line measured at the half-maximum intensity, λ (0.154 nm) and θ denotes the wavelength of the X-rays and the Bragg diffraction angle, respectively. The correction for instrumental broadening is taken into consideration in the measurement of the peak broadening by comparing the widths at half-maximum intensity of X-ray reflection between the sample and the single crystalline Si standard, and then Gaussian correction is used to remove the instrumental broadening to obtain the true crystal broadening:

$$B_p^2(2\theta) = B_h^2(2\theta) - B_f^2(2\theta)$$

where $B_p(2\theta)$ is the true half-maximum width; $B_h(2\theta)$ and $B_f(2\theta)$ are the half-maximum widths of the sample and the single crystalline Si standard, respectively.[25] The theta values of $2\theta = 30^\circ$ is selected to calculate the crystallite size, the peaks belong to ZrO_2. The calculated average grain size is 61 nm for the as-sprayed coating, and is 63, 110 and 120 nm after annealing at 1100 °C for 25, 100 and 300 h, respectively. The grain size of nanostructured 13AlYSZ coating increases as the annealing time increases.

Fig. 4 represents a comparison of the grain size of the as-sprayed nanostructured 13AlYSZ and nanostructured YSZ coating. Without the nanostructured Al_2O_3 doping, the ZrO_2 particle grain size is increased from 57 nm before annealing to 178 nm when annealing at 1100 °C for 300 h[16] and the 13AlYSZ particle grain size varies from 61 to 120 nm. It implies that the addition of nano-Al_2O_3 inhibits effectively the grain growth of nanostructured ZrO_2.

Fig. 5 shows the polished cross-section of as-sprayed nanostructured 13AlYSZ coating before (a) and after annealing at 1100 °C for 25 h (b), 100 h (c) and 300 h (d) at low magnification, and (e)–(h) is at the high magnification corresponding to annealing at 1100 °C for 0, 25, 100 and 300 h. As shown in Fig. 5, the observed microstructure is typical of APS nanostructured coatings with nanozones (unmelted or partially melted particles), splats, microcracks and high volume spheroidal pores. The volumetric fractions of spheroidal pores are reduced for longer heat treatment (Fig. 5(a)–(d)). During spraying, the nanostructured 13AlYSZ particles are injected into the plasma plume and some of the particles are completely molten. When the molten particles impact the substrate surface with a high velocity, the flattening and solidification of the liquid particles occur. As the result, hundreds of splats are overlapped to form a thin coating (Fig. 5(e)–(h)). Simultaneously, non-molten and partially molten particles also impact the surface. However, the flattening of those particles is not completed because the wetting is not good enough due to its low local temperature. Some small pores are formed between the deposited splats because the intersplat contact is not good. On the other hand, gas could not completely release from the splats or lamellae. Some globular pores are formed within the coating. After sintering at 1100 °C for increased hours, the grain size of unmelted or semi-melted particles increases, leading to the densification of the nanozones and the reduction of porosity.

The fractured cross-section morphologies of the as-sprayed nanostructured 13AlYSZ coatings before and after heating treatment at 1100 °C for 25, 100 and 300 h are performed in Fig. 6. There are three main types of microstructural features that coexist in the coating: (i) dense area (melted area), (ii) nanozones (unmelted or partially melted particles), and (iii) porosity. With the annealing treatment time increasing from 25 to 300 h, the nanostructured 13AlYSZ coatings becomes denser and the unmelted particles of the nanozones grow gradually.

To further probe the grain growth of the nanostructured 13AlYSZ coatings after annealing treatment at 1100 °C for different times, TEM images of the nanostructured 13AlYSZ TBCs after annealing treatment at 1100 °C for 25, 100 and 300 h are shown (Fig. 7). From Fig. 7, it was seen that the average grain size is increased from 63 to 120 nm with the heat-treatment time varying from 25 to 300 h, which is in accordance with the XRD results calculated using Scherrer equation.

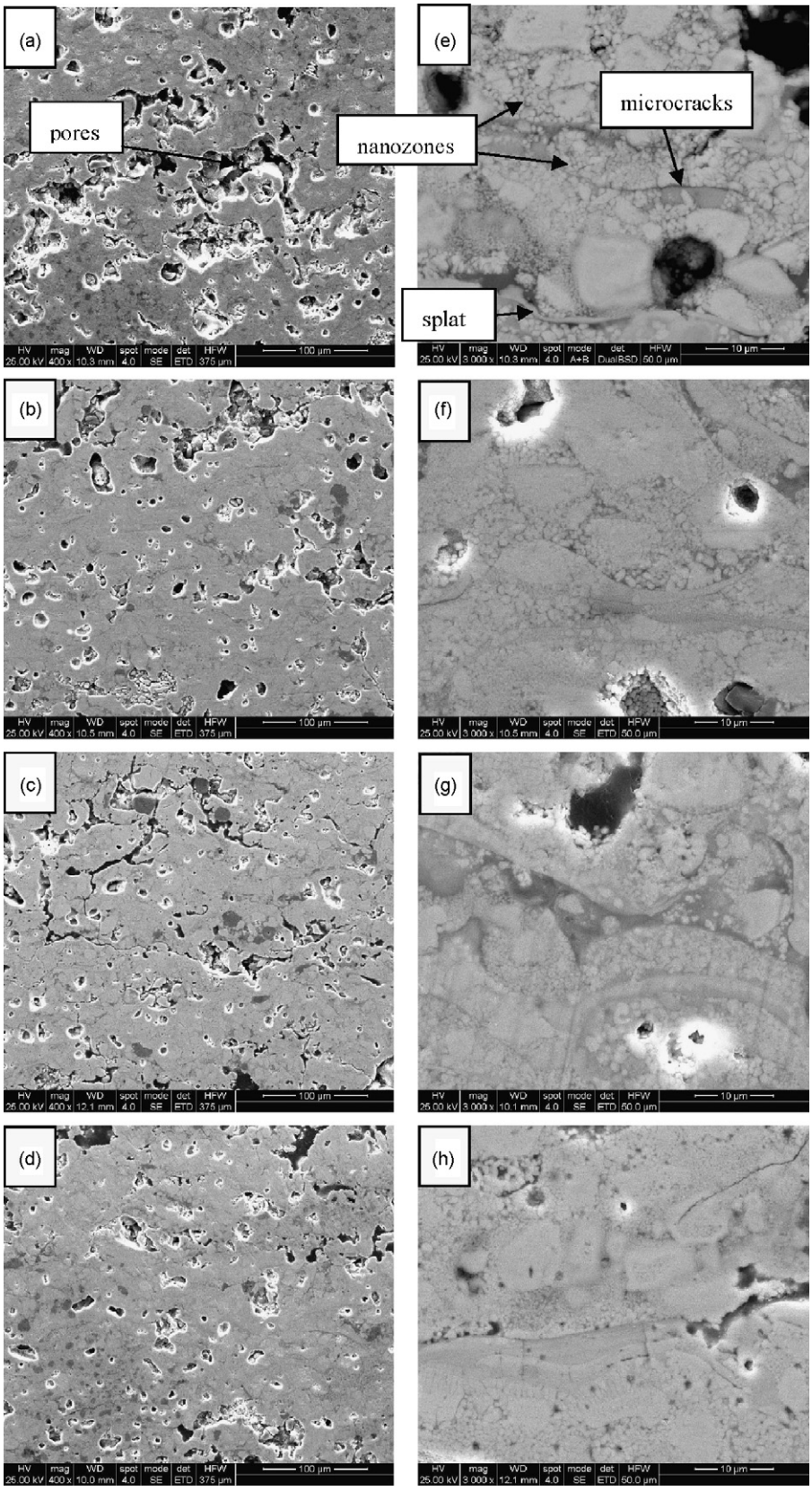

Fig. 5. The polished cross-section of as-sprayed nanostructured 13AlYSZ coating before (a) and after annealing at 1100 °C for 25 h (b), 100 h (c) and 300 h (d) at low magnification, and (e)–(h) is at the high magnification corresponding to annealing at 1100 °C for 0, 25, 100 and 300 h.

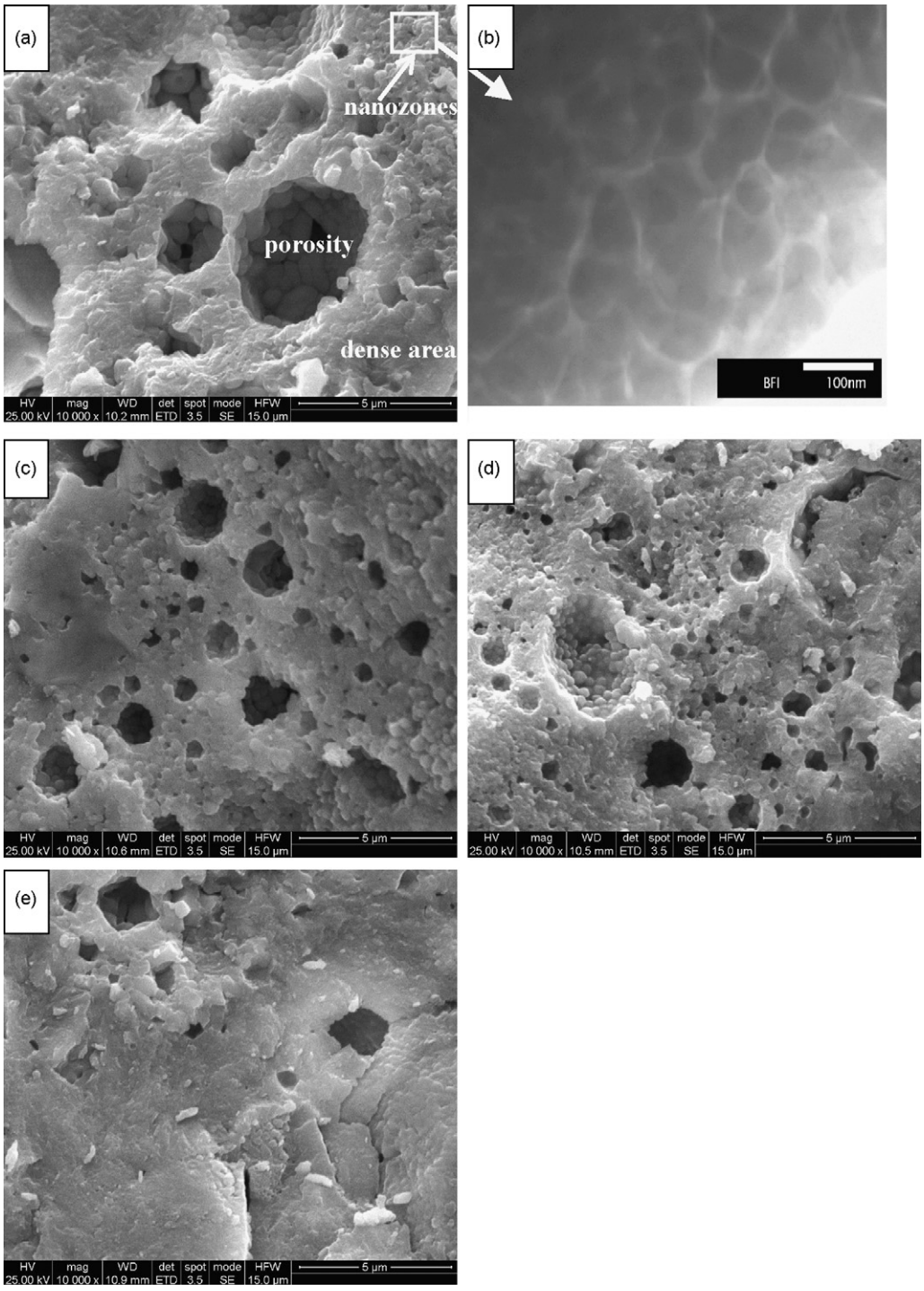

Fig. 6. Fractured cross-section morphologies of nanostructured 13AlYSZ coatings before (a) and after heating treatment at 1100 °C for 25 h (b), 100 h (c) and 300 h (d). (A) shows magnified views of framed regions in (a) with TEM.

In order to investigate the microstructure and composition of 13AlYSZ coatings after annealing treatment at 1100 °C for 100 h, the TEM image and EDXS spectra of the nanostructured 13AlYSZ TBCs after annealing treatment at 1100 °C for 100 h is shown (Fig. 8). Actually, Al_2O_3 content is about 20 vol.% equivalent to 13 wt% of Al_2O_3 in 8YSZ matrix. In Fig. 8(a), Al_2O_3 content appears to be ~30 vol.%, which is caused by the small area selected for the TEM micrograph of 13 AlYSZ coating. As confirmed by the selected area electron diffraction patterns (SAEDPs) in Fig. 8(b) and (c), the coatings are composed of t-ZrO_2 and α-Al_2O_3 phase using zone axis [0 0 1] and [1 1 $\bar{2}$ 3], respectively. According to the EDXS spectra in Fig. 8(d) and (e), the chemical composition (atomic basis) of "m" region is Zr/Al/Y = 48/2/4 and the chemical composition of "n" region is

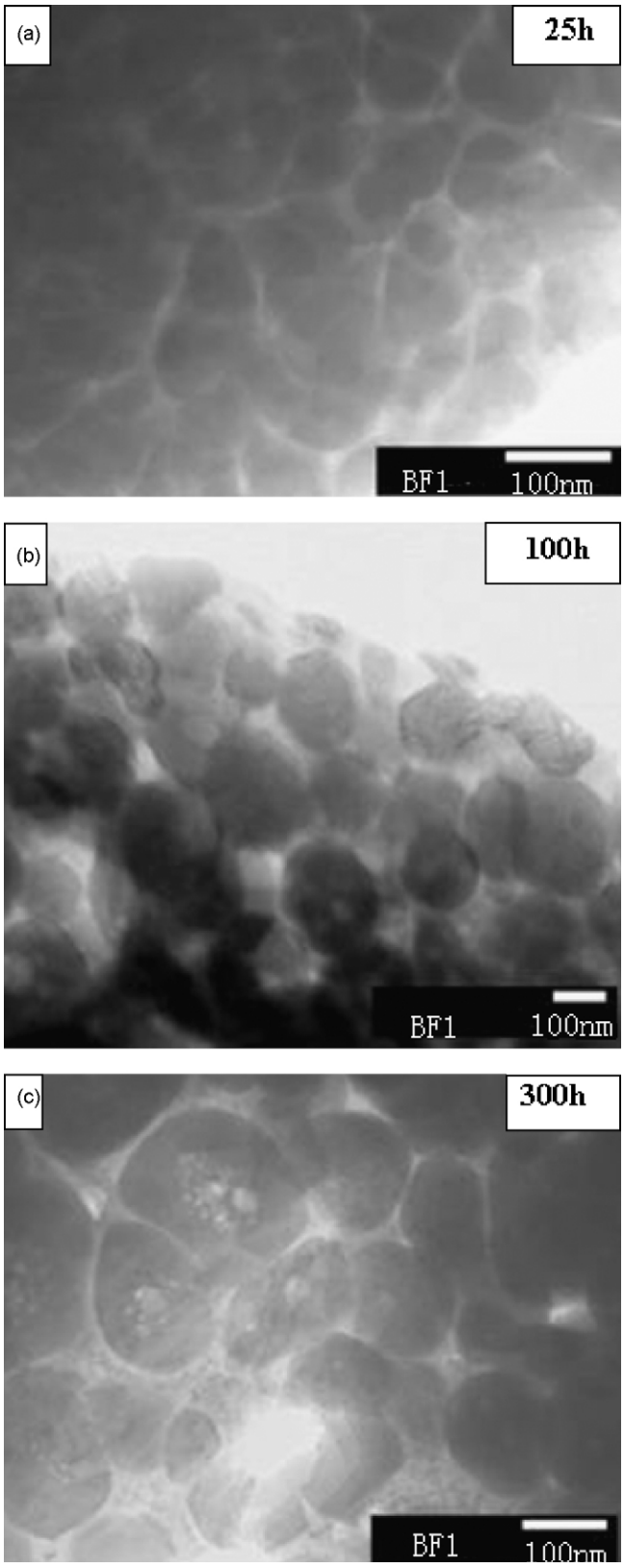

Fig. 7. TEM images of the nanostructured 13AlYSZ TBCs after annealing treatment at 1100 °C for 25 h (a), 100 h (b) and 300 h (c).

Zr/Al/Y = 7/31/1. It implies that the area "m" is mainly composed of t-ZrO_2, and area "n" is mainly composed of α-Al_2O_3. It is revealed by Fig. 8 that some α-Al_2O_3 phases are clamped by the two neighboring ZrO_2 grains forming the intragranular structure (as marked "A" in Fig. 8(a)) and some are located along grain boundary of nanostructured ZrO_2 (marked "B" in Fig. 8(a)).

3.3. Porosity variation of as-sprayed nanostructured 13AlYSZ coatings with the heat-treatment time

Fig. 9 shows the cumulative porosity distribution of the free-standing coating specimens that is determined by mercury porosimetry (MP). Cumulative porosity is the pore content normalized to the volume of the sample. Before the measurement, specimen surfaces were finely polished in order to minimize the effect of surface roughness to the porosity measurement. In Fig. 9, it is clearly shown that the sintering of the coating leads to a lower porosity, as the annealing treatment time increased from 0 to 300 h, the cumulative porosity decreased from 23.8 to 18%. The porosity is composed of micropores (diameter < 4 μm) and macropores (diameter > 4 μm). The presence of macropores above 4 μm in the coating reduced from 5.9 to 5.8% after heat treatment at 1100 °C from 0 to 300 h, which does not change much. But the micropores below 4 μm reduced from 17.8 to 12.2% after annealing at 1100 °C from 0 to 300 h. Sintered sample after 100 h heat treatment has higher number of small pores up to 17% than 25 h of 14% sintered sample. The radius of pores below 4 μm have a significant effect on the cumulative porosity. According to Guo et al.,[26,27] the larger defects corresponding to radius above 1 μm are believed to have resulted from macrocracks and voids (globular and irregular pores). The fine pores with a size smaller than 1 μm are mainly attributed to microcracks such as intersplat gaps and intrasplat cracks. The pores of the nanostructured 13AlYSZ coatings are much larger than that of traditional TBCs. The thermal insulation is dependent not only on the total porosity but also on the aspect ratio of pores. Those microcracks or gaps normal to heat flow make a larger contribution to lowering the conductivity although the percentage of such kinds of microcracks or gaps is not as higher as those of globular pores. In terms of porosity measurements, the microcracks or gaps with the size of smaller than 4 μm exhibited a larger reduction than those large pores did. Therefore, after sintering, the coating yielded a considerable reduction in thermal insulation.

4. Discussions

As shown in Figs. 4 and 7, with the increasing of the annealing treatment time from 25 to 300 h, the ZrO_2 particle grain size is changed from 63 to 120 nm. The addition of nano-Al_2O_3 effectively inhibits the grain growth of nanostructured ZrO_2, and during the heating treatment process, the nanostructured ZrO_2 particles grow faster than the nano-Al_2O_3 particles. The addition of nano-Al_2O_3 effectively inhibits the grain growth of nanostructured ZrO_2 during the heat-treatment process, which can be explained as follows.

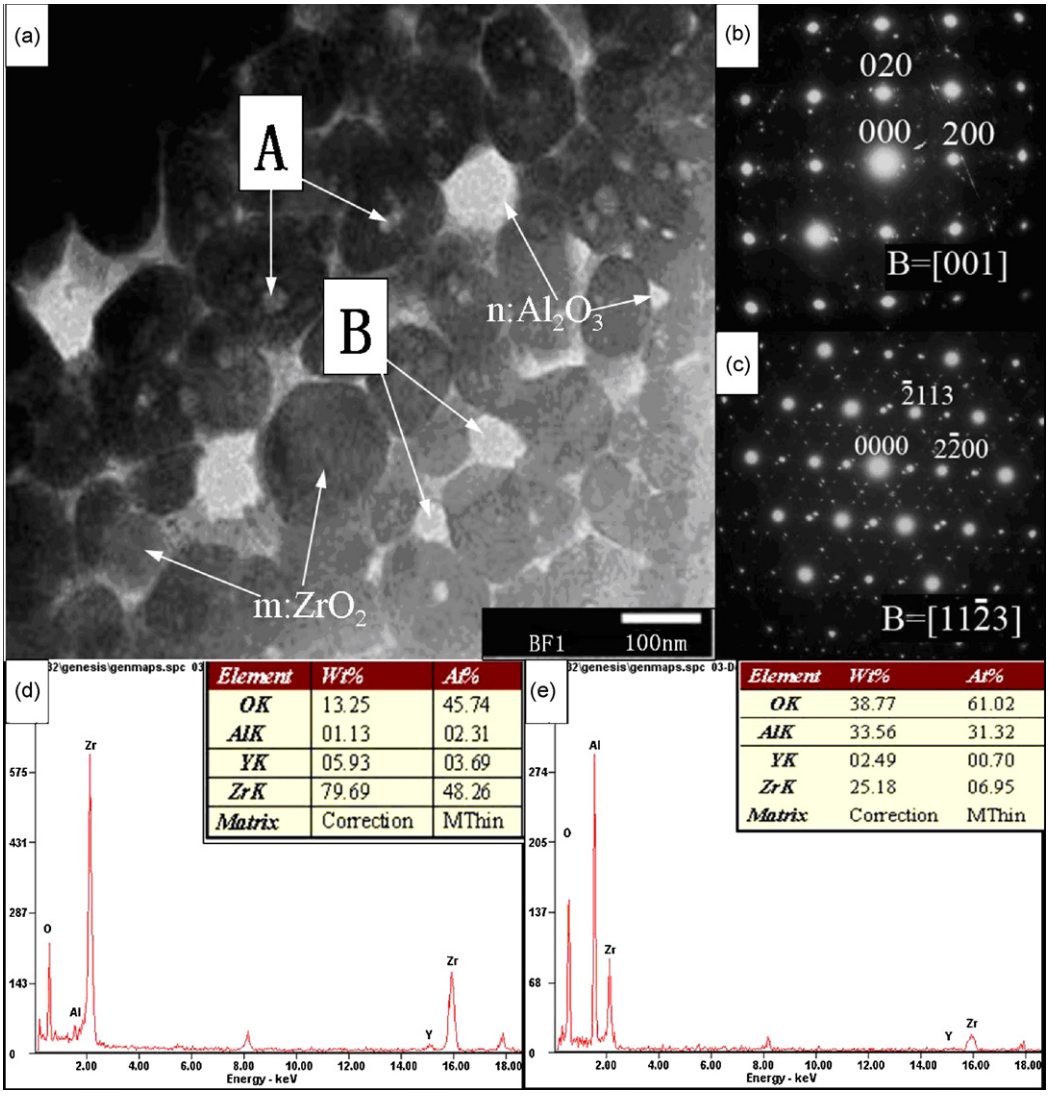

Fig. 8. Bright-field TEM images (a) and corresponding indexed SAEDPs ((b) and (c)) of as-sprayed 13AlYSZ coatings after heat treatment at 1100 °C for 100 h and the EDXS spectra in (d) and (e) correspond to the Zr-rich and the Al-rich regions.

At the beginning of annealing treatment, the nanostructured ZrO_2 grains are rather small and dispersed homogeneously, and the Al element is in solid solution with ZrO_2 or in the amorphous intergranular pocket at triple junction. The Al-depleted nature of the t-ZrO_2 grains surrounding the α-Al_2O_3 precipitates in the heat-treated coating indicates that the precipitation of the α-Al_2O_3 occurs as a result of the outward diffusion of the Al that is in solid solution with ZrO_2 or detachment from the Al-rich amorphous phase.[15] The second-phase Al_2O_3 tends to move and gather along the ZrO_2 boundaries. When the migration speed of the second phase is less than that of the ZrO_2, they are partly clamped by the two neighboring ZrO_2 grains, forming the intragranular structure[28] (marked "A" in Fig. 8(a)). And some of the nanostructured Al_2O_3 particles are pushed and squeezed by ZrO_2 grains during grain boundary migration, locating along grain boundary of nanostructured ZrO_2 and pinning the grain boundaries (marked "B" in Fig. 8(a)).

The mechanism of the intragranular structure inhibiting the grain growth can be explained from the viewpoint of the sur-

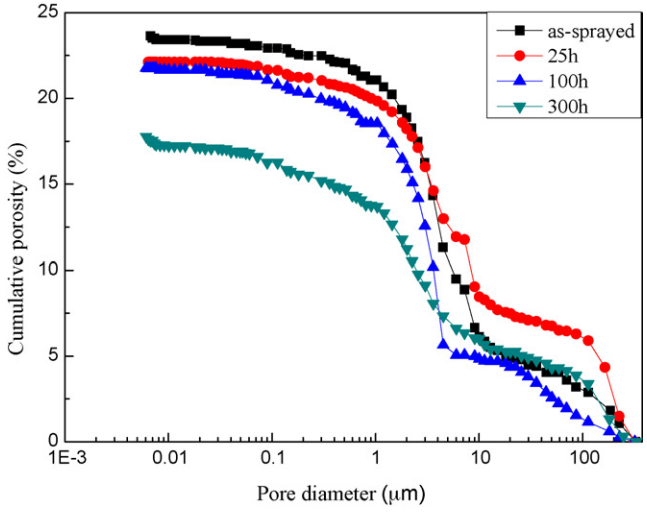

Fig. 9. The cumulative porosity variation of the nanostructured 13AlYSZ coating before and after heat treatment at 1100 °C for 25, 100 and 300 h.

face tension equilibrium between two phases. When the two neighboring ZrO_2 phase are encountered with the nanostructured Al_2O_3 particles, the grain boundaries of the ZrO_2 particles penetrate through the Al_2O_3 particles. The Al_2O_3 inclusions are dragged by ZrO_2 grain boundaries that have sufficient interface energy, each of which can independently satisfy the equilibrium surface tension required at the particle interface. The ZrO_2 grains finally coalesce together to form the intragranular structure. Detachment from the particle can only occur when the two major ZrO_2 boundaries rotate by 180°, which effectively inhibits the grain growth and results in the stabilization of grains.

The particles located along the grain boundaries also contribute to inhibiting the grain growth of the ZrO_2 particles. The large second-phase particles pin the grain boundaries. Such pinning effect is in harmony with Zener effect where the particles pinning the grain boundaries is much smaller than the average grain size of the matrix. It is attributed to the coalescence or clustering of the small contiguous particles at triple junctions. This phenomenon alters the topology of grains, subsequently alters the grain growth kinetics through changes in shape and local boundary curvature. The grains of matrix and the second-phase particles mutually constrain one another in this way, and then the grain growth of the faster growing species will be limited by the rate at which the slower growing phase coalescence or clustering.[29]

The sintering resistance of the 13AlYSZ coating can be understood by the shrinkage of the porosity. During the sintering process, due to the presence of nanostructured particles and porosity, the porous nanozones is under a higher driving force for sintering and densification,[7] which leads to a fast sintering. Therefore, the nanozones tend to densify at fast rates and the porosity of the coating decreased from 23.8 to 22.1% after annealing treatment for 25 h. With the annealing treatment ongoing, the velocity of sintering is suppressed, and the porosity dropped to 21.8% after annealing treatment for 100 h. This is caused by the grain growth and the precipitation of Al_2O_3. The grain growth leads to a lower driving force for sintering and the precipitation of Al_2O_3 pins the boundaries and therefore made sintering difficult. When the annealing time increases to 300 h, the porosity decreased to 18%. The slightly greater reduction in porosity per unit time in going from 100 to 300 h may be simple experimental error since it is very difficult to measure the porosity level in a coating very accurately. Usually, an accelerated sintering tends to occur in the early stage, i.e. 25 h in this work, because the initial higher porosity and finer particle sizes contributed to sintering. As a result, an apparent shrinkage is observed in the stage. In this study, about 6% porosity decreased in the sintering process, which is similar to the tendency for the sintering of traditional 7 wt% Y_2O_3–stabilized ZrO_2 ceramic coating.[30]

In summary, the intragranular structure and the second Al_2O_3 phase located in the grain boundaries of the ZrO_2 phase effectively inhibited the grain growth of nanostructured ZrO_2. With the prolongation of the annealing treatment, the porosity of the coatings decreased from 23.8 to 18%. In the meantime, effect of heat treatment on the thermo-physical properties need to be investigated in the future study.

5. Conclusions

Nanostructured 13 wt% Al_2O_3–8 wt% Y_2O_3–ZrO_2 coatings were prepared by atmospheric plasma spraying. In the as-sprayed coating, the Al element is in solid solution with ZrO_2. After heat treatment for about 100 h, the Al_2O_3 is precipitated. The addition of nano-sized Al_2O_3 effectively inhibits the grain growth of the ZrO_2 phase. The effect is attributed to the formation of the intragranular structure and constraining the grain boundaries of nanostructured ZrO_2. The porosity of the coatings decreased from 23.8 to 18% after sintering at 1100 °C for 300 h. The addition of Al_2O_3 improves the sintering resistance of the YSZ coatings.

Acknowledgements

This work is supported by the National Natural Science Foundation of China, the Aviation Science Foundation of 2008ZE51073, Program for New Century Excellent Talents in University (NCET) and Program for Changjiang Scholars and Innovative Research Team in University (IRT0512).

References

1. Padture, N. P., Gell, M. and Jordan, E. H., Thermal barrier coatings for gas-turbine engine applications. *Science*, 2002, **296**, 280.
2. Aygun, A., Vasiliev, A. L. and Padture, N. P., Novel thermal barrier coatings that are resistant to high-temperature attack by glassy deposits. *Acta Mater.*, 2007, **55**, 6734.
3. Ercan, B., Bowman, K. J. and Trice, R. W., Effect of initial powder morphology on thermal and mechanical properties of stand-alone plasma-sprayed 7 wt.% Y_2O_3–ZrO_2 coatings. *Mater. Sci. Eng. A*, 2006, **435–436**, 212.
4. Xie, L. D., Chen, D. Y. and Jordan, E. H., Formation of vertical cracks in solution-precursor plasma-sprayed thermal barrier coatings. *Surf. Coat. Technol.*, 2006, **201**, 1058.
5. Shanmugavelayutham, G. and Kobayashi, A., Mechanical properties and oxidation behaviour of plasma sprayed functionally graded zirconia–alumina thermal barrier coatings. *Mater. Chem. Phys.*, 2007, **103**, 283.
6. Jang, B. K. and Matsubara, H., Influence of porosity on thermophysical properties of nano-porous zirconia coatings grown by electron beam-physical vapor deposition. *Scripta Mater.*, 2006, **54**, 1655.
7. Lima, R. S. and Marple, B. R., Nanostructured YSZ thermal barrier coatings engineered to counteract sintering effects. *Mater. Sci. Eng. A*, 2008, **485**, 182.
8. Chen, H., Zhou, X. M. and Ding, C. X., Investigation of the thermomechanical properties of a plasma-sprayed nanostructured zirconia coating. *J. Eur. Ceram. Soc.*, 2003, **23**, 1449.
9. Gell, M., Application opportunities for nanostructured materials and coatings. *Mater. Sci. Eng. A*, 1995, **204**, 246.
10. Racek, O. and Berndt, C. C., Mechanical property variations within thermal barrier coatings. *Surf. Coat. Technol.*, 2007, **202**, 362.
11. Liang, B. and Ding, C. X., Nanostructured zirconia coating prepared by atmospheric plasma spraying. *Surf. Coat. Technol.*, 2005, **197**, 185.
12. Zhou, C. G., Wang, N. and Wang, Z. B., Thermal cycling life and thermal diffusivity of a plasma-sprayed nanostructured thermal barrier coating. *Scripta Mater.*, 2004, **51**, 945.
13. Jang, B. K., Thermal conductivity of nanoporous ZrO_2–4 mol% Y_2O_3 multilayer coatings fabricated by EB-PVD. *Surf. Coat. Technol.*, 2008, **202**, 1568.
14. Zhou, C. G., Wang, N. and Xu, H. B., Comparison of thermal cycling behavior of plasma-sprayed nanostructured and traditional thermal barrier coatings. *Mater. Sci. Eng. A*, 2007, **452–453**, 569.

15. Vasiliev, A. L., Padture, N. P. and Ma, X. Q., Coatings of metastable ceramics deposited by solution-precursor plasma spray. I. Binary ZrO_2–Al_2O_3 system. *Acta Mater.*, 2006, **54**, 4913.
16. Wang, N., Zhou, C. G. and Gong, S. K., Heat treatment of nanostructured thermal barrier coating. *Ceram. Int.*, 2007, **33**, 1075.
17. Raghavan, S., Wang, H. and Dinwiddie, R. B., The effect of grain size, porosity and yttria content on the thermal conductivity of nanocrystalline zirconia. *Scripta Mater.*, 1998, **39**, 1119.
18. Yang, H. S., Bai, G. R., Thompson, L. J. and Eastman, J. A., Interfacial thermal resistance in nanocrystalline yttria stabilized zirconia. *Acta Mater.*, 2002, **50**, 2309.
19. Suwa, Y., Saito, Y. and Onodera, H., Phase field simulation of grain growth in three dimensional system containing finely dispersed second-phase particles. *Scripta Mater.*, 2006, **55**, 407.
20. Wang, X., Tian, J., Yu, X. G., Shan, Y., Liu, Z. F. and Yin, Y. S., Effect of microstructure on the fracture behavior of micro–nano ZTA composite. *Mater. Chem. Phys.*, 2008, **112**, 213.
21. Liang, B., Liao, H. L., Ding, C. X. and Coddet, C., Nanostructured zirconia–30 vol.% alumina composite coatings deposited by atmospheric plasma spraying. *Thin Solid Films*, 2005, **484**, 225.
22. Matsunoto, M., Aoyama, K., Matsubara, H. and Takayama, K., Thermal conductivity and phase stability of plasma sprayed ZrO_2–Y_2O_3–La_2O_3 coatings. *Surf. Coat. Technol.*, 2005, **194**, 35.
23. Klug, H. P. and Alexander, L. E., *X-ray Diffraction Procedures for Polystalline and Amorphous Materials*. John Wiley & Sons, Inc., London, 1954, p. 138.
24. Shaw, L. L. and Goberman, D., The dependency of microstructure and properties of nanostructured coatings on plasma spray conditions. *Surf. Coat. Technol.*, 2000, **130**, 1.
25. Zhou, H., He, B., Wang, J. and Sun, B. D., Nanostructured yttria stabilized zirconia coatings deposited by air plasma spraying. *Trans. Nonferr. Met. Soc. China*, 2007, **17**, 389.
26. Guo, H. B., Kuroda, S. and Murakami, H., Microstructures and properties of plasma-sprayed segmented thermal barrier coatings. *J. Am. Ceram. Soc.*, 2006, **89**, 1432.
27. Guo, H. B., Murakami, H. and Kuroda, S., Effect of hollow spherical powder distribution on porosity and segmentation cracks in thermal barrier coatings. *J. Am. Ceram. Soc.*, 2006, **89**, 3797.
28. Xu, C. H. and Sun, D. M., Formation of intragranular nano-structures in micro-sized ceramic composite materials. *Mater. Sci. Eng. A*, 2008, **491**, 338.
29. Alexander, K. B., Becher, P. F., Waters, S. B. and Bleier, A., Grian growth kinetics in alumina–zirconia (CeZTA) composites. *J. Am. Ceram. Soc.*, 1994, **77**, 939.
30. Siebert, B., Funke, C., Vaβen, R. and Stover, D., Changes in porosity and Young's modulus due to sintering of plasma sprayed thermal barrier coatings. *J. Mater. Process. Technol.*, 1999, **92–93**, 217.